Metal Oxides

DOI: 10.1002/ange.201104029

Enabling the Anodic Growth of Highly Ordered V_2O_5 Nanoporous/Nanotubular Structures**

*Yang Yang, Sergiu P. Albu, Doohun Kim, and Patrik Schmuki**

In 1995 Masuda and Fukuda demonstrated that highly ordered, self-organized porous alumina structures can electrochemically be grown by anodizing aluminium in an oxalic acid electrolyte under a set of optimized electrochemical conditions.[1] This initiated a large amount of follow-up work that used these structures either directly (e.g. as filters or photonic materials) or indirectly as a template for the deposition of a wide range of materials as nanowires, nanorods, or nanotubes.[2] Self-organized porous oxide growth was believed to be constrained to alumina, until in 1999 Zwilling et al. introduced the growth of self-organized TiO_2 nanotubes from Ti electrodes when anodized in a fluoride-containing electrolyte.[3] In the following years, the "dilute" fluoride-based electrolytes were refined, not only to allow for an ever increasing control of the TiO_2 nanotube geometry,[4] but dilute fluoride solutions were also found to be extremely versatile to grow highly ordered anodic nanotubes or nanoporous layers on other metals such as Zr, Hf, Nb, Ta, and a wide range of alloys.[5] Common to all these anodic oxide growth procedures is that water is used as a source for oxide formation and fluorides are used to solubilized excess cations—this establishes a formation–dissolution steady-state situation. To achieve self-organizing oxide tubes or pore-growth conditions, the H_2O and F^- contents in the electrolyte need to be optimized. A difficulty is that the dilute fluoride solutions also lead to chemical etching of the generated oxide structure, that is, for optimized conditions the chemical resistance of the formed oxide against fluoride and H_2O etching may become crucial. This is no problem for oxides such as Ta_2O_5 or Nb_2O_5 (and only mildly for TiO_2), but an extremely high etching susceptibility prevented (in spite of many attempts) the growth of defined ordered anodic layers from one of the most important transition-metal oxides, V_2O_5. Here, we show how to overcome this problem by using complex fluoride electrolytes such as $[BF_4]^-$ or $[TiF_6]^{2-}$, which allow for the first time, to successfully grow self-organized nanoporous and nanotubular V_2O_5 structures.

[*] Dr. Y. Yang, S. P. Albu, Dr. D. Kim, Prof. Dr. P. Schmuki
Department of Materials Science and Engineering, WW4-LKO
University of Erlangen-Nuremberg
Martensstrasse 7, 91058 Erlangen (Germany)
E-mail: schmuki@ww.uni-erlangen.de
Homepage: http://www.lko.uni-erlangen.de

[**] This work was supported by grants from the DFG and the Alexander von Humboldt Foundation of Germany (Y.Y.). The authors acknowledge Ulrike Marten-Jahns and Helga Hildebrand for the XRD and XPS measurements.

Supporting information for this article is available on the WWW under http://dx.doi.org/10.1002/anie.201104029.

This is of special significance as V_2O_5 is one of the most investigated transition-metal oxides because of its application in catalysis, lithium batteries, electrochromics, and sensors.[6] For many of these applications nanoscale geometries bear significant advantages in view of electronic, magnetic, catalytic, and ion intercalation properties.[7] Up to now the synthesis of V_2O_5 nanotubes was mainly achieved by hydrothermal treatments, which yield randomly oriented assemblies (a nanotube powder).[8]

The key challenge for the preparation of self-organized V_2O_5 nanotubes or any vanadium oxide by electrochemical techniques is the instability of vanadium oxide in any water-containing electrolyte and the ease of formation of highly soluble complexes with a wide range of anions. Some work has shown the feasibility to grow compact layers or films of anodic vanadium oxide in specific nonaqueous electrolytes.[9] But over the past few years numerous attempts failed to anodically grow V_2O_5 nanotubes or ordered porous layers.[10] Virtually any electrolyte that is typically used for fabricating other transition-metal oxide nanotubes or ordered pore arrays was explored but failed (an overview of such attempts is compiled in the Supporting Information, Table S1). Here, we demonstrate that using complex fluoride salt electrolytes such as $[TiF_6]^{2-}$ and $[BF_4]^-$ enable self-organized anodization.

In a first approach, we formed $[TiF_6]^{2-}$ species by dissolving pure titanium in HF and then dissolving this solution in ethylene glycol which was then used for anodization. After parameter screening for the dissolved Ti content, HF concentration, water content, and applied voltage we established conditions to grow highly ordered nanoporous and nanotubular vanadium oxide structures as shown in Figure 1. The vertically aligned vanadium oxide nanoporous layer shown in Figure 1a has a thickness of 13 μm and a pore diameter around 15 nm and was fabricated by anodization of a vanadium foil in an ethylene glycol (EG) containing 0.2 M HF and 300 ppm Ti electrolyte at 120 V for 2 h. By extending the anodization duration to 24 h, a tubular structure as shown in Figure 1b can be formed (the top-view SEM images of typical tubular structures versus porous structures are given in Figure S1 in the Supporting Information). From the thickness–time curve shown in Figure 2a, it is found that a steady increase of oxide growth takes place and, for example, after 12 h of anodization a highly ordered nanoporous/tubular layer of approximately 45 μm thickness can be achieved (see Figure S2 in the Supporting Information). The growth rate of the porous layer becomes slower with extended anodization duration, which is a typical for self-organized anodic layers.[11]

We investigated the influence of the $[TiF_6]^{2-}$ concentration in the range from 200 (equivalent to 4.7 mM $[TiF_6]^{2-}$) to 1500 ppm Ti (equivalent to 35 mM $[TiF_6]^{2-}$). An etched layer

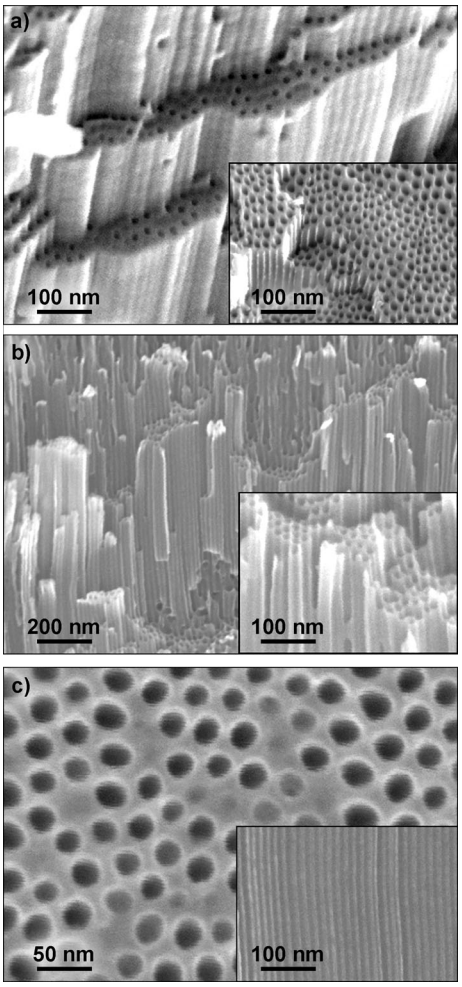

Figure 1. a) SEM images of the nanoporous V_2O_5 layer anodically grown in $[TiF_6]^{2-}$ electrolyte (300 ppm Ti, 0.2 M HF, EG) for 2 h. b) SEM images of V_2O_5 with tubular structure anodically grown in $[TiF_6]^{2-}$ electrolyte for 24 h, and c) nanoporous V_2O_5 layer anodically grown in $[BF_4]^-$-containing electrolyte (14 mM $NaBF_4$, 3 M H_2O, EG). The inset in (a) shows a surface SEM image, whereas the insets in (b) and (c) show cross-section SEM images.

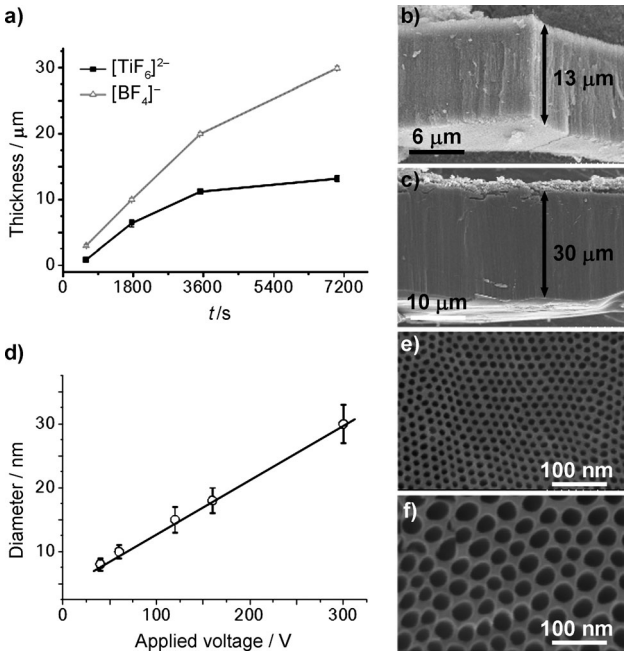

Figure 2. a) Time–thickness curves of nanoporous V_2O_5 layers anodically grown in $[TiF_6]^{2-}$ and $[BF_4]^-$-containing electrolytes (squares: 300 ppm Ti electrolyte dissolved in EG, triangles: 14 mM $NaBF_4$ electrolyte with 3 M H_2O in EG). b,c) SEM images of the porous layers anodically formed in $[TiF_6]^{2-}$ and $[BF_4]^-$-containing electrolytes at 120 V for 2 h, respectively. d) Applied voltage–diameter curve of the porous layer anodically grown in Ti (300 ppm) electrolyte. e,f) SEM images of the porous layers formed at 40 and 300 V, respectively.

with a poorly-defined porous structure was obtained for concentrations below the optimum (see Figure S3 in the Supporting Information). The quality of the porous layer decreases and partly etching of the porous layer takes place (see Figure S4 in the Supporting Information) when the concentration is above the optimum. Self-ordered growth is limited to highly optimized electrolyte concentration conditions. In control experiments, HF concentration and water content in the electrolyte were investigated (see Figure S5 in the Supporting Information). The results demonstrate that addition of HF or water to the electrolyte leads to etching and dissolution of the porous layer. Also any attempts to use "aged" electrolytes or electrolyte containing V-fluoride species failed (see Figures S6a and S6b in the Supporting Information). For the successful preparation of all layers it should also be noted that the "as-formed" anodic V_2O_5 layer is hygroscopic and adsorption of moisture from air leads to a quick decay of the structure (see Figure S6c–6f in the Supporting Information), that is, a fast transfer to a dry box or annealing is required to keep the structures stable.

As for other anodic porous oxide layers, the applied voltage is an important factor to control the pore diameter.[12] As shown in Figure 2b the pore diameter for the ordered V_2O_5 layers increases linearly with the applied voltage. To confirm that the key role for enabling V_2O_5 self-organized oxide growth is indeed the $[TiF_6]^{2-}$ complex, we performed additional experiments and gave directly 7 mM $(NH_4)_2TiF_6$ to 0.1M HF. In such a $(NH_4)_2TiF_6$-containing electrolyte V_2O_5 porous layers are grown as well (see Supporting Information Figure S7a). To generalize the approach, we tested the feasibility of the $[BF_4]^-$ complex, namely in the form of NH_4BF_4 and $NaBF_4$ (ethylene glycol with 14 mM NH_4BF_4 or $NaBF_4$ electrolyte and 3 M H_2O; additional experiments are shown in Figure S7b in the Supporting Information). Figures 1c and 2c show that also in this system highly ordered V_2O_5 nanoporous layers with an average pore diameter of 10 nm can be anodically formed up to thickness of several 10 μm. The thickness–time curve of porous layers grown in $[BF_4]^-$-containing electrolytes (Figure 2a) also shows a trend similar to that of layers produced in $[TiF_6]^{2-}$.

The chemical composition of the samples was examined by energy dispersive X-ray (EDX) and X-ray photoelectron spectroscopy (XPS) at different stages of the experiment, that is, immediately after anodization, after soaking in ethanol

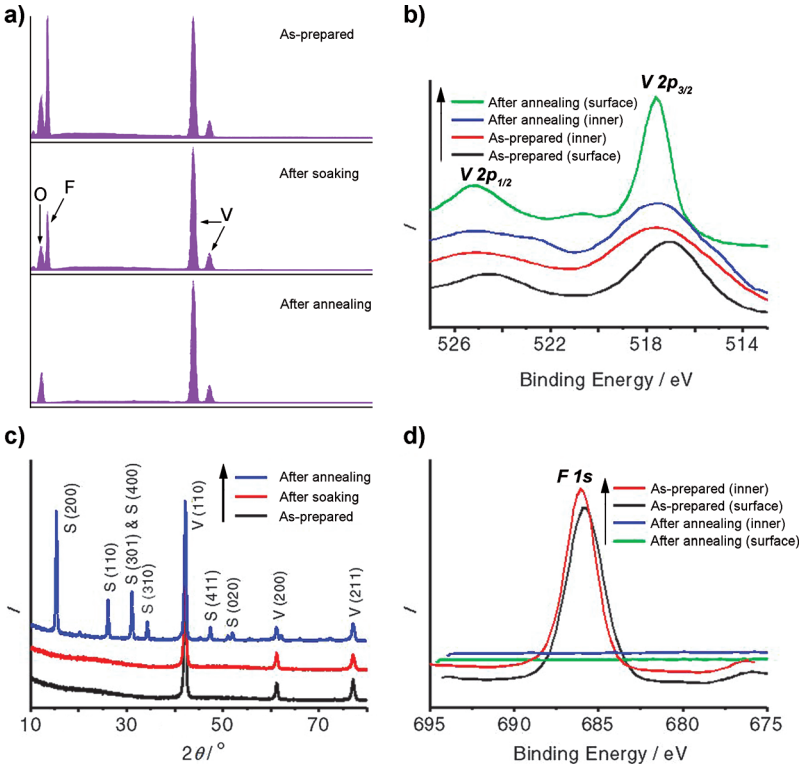

Figure 3. a) EDX spectra obtained after different treatments. b,d) XPS analysis on both the surface of the layer as well as the inner porous structure (the X-ray photoelectron spectra of the inner porous structure were obtained after sputtering in the sample, 100 nm deep), c) XRD pattern of the nanoporous layer before and after soaking and after annealing at 200 °C (S-orthorhombic phase of V_2O_5, V: vanadium substrate).

overnight and after annealing at 200 °C. It is evident that high amounts of fluorides are present on the surface of the layer as well as in the porous structure (Figure 3 a and Figure S8 in the Supporting Information). These fluoride compounds are gradually removed by soaking in ethanol and then totally eliminated after heat treatment at 200 °C. The finding of very high fluoride contents through the entire as-formed sample confirms that during anodization permanently fluorides are embedded in the oxide structures. XPS was also used to evaluate the chemical composition of the as-prepared sample and the sample after annealing at 200 °C for 3 h. Vanadium is present in all samples with peaks of binding energies around 517.54 eV for $V2p_{3/2}$ and 525.03 eV for $V2p_{1/2}$, respectively, which can be assigned to V^{5+}.[13] Fluorine is only present in the sample before annealing with a binding energy around 685.84 eV. The results of EDX and XPS agree well. Additionally, X-ray diffraction (XRD) techniques were used to investigate the crystal structure of the porous vanadium oxide layer. Before the sample was annealed we did not observe peaks assigned to crystalline vanadium oxides, which indicates an amorphous oxide layer. The porous layer crystallizes as orthorhombic V_2O_5 phase after annealing at 200 °C for 3 h (Figure 3 c). The crystallization temperature of a porous V_2O_5 layer is considerably lower relative to bulk V_2O_5 (the crystallization temperature is around 300 °C) possibly because of the specific structure of the porous layer or size effects on the nanoscale.[14] Furthermore, neither EDX, XPS, and XRD show Ti uptake in the porous layer in any form, that is, not $[TiF_6]^{2-}$ as such is embedded in the structure or forms an absorbed or precipitated layer of vanadium (oxide) but F^- species interact with vanadium (oxide).

The special role of complex fluoride ions may be that they form comparably stable fluoride adducts with VO_2^+ ions and promote the formation of VO_x–F_y adducts as reported recently for solutions containing $[BF_4]^-$.[15] After formation of the nanotubes/channels the outer part of the nanotubes/channels is mainly composed of a vanadium oxide–fluoride adduct, which is not stable in water or adsorbs moisture from air.[16] Only after annealing this layer of vanadium oxide–fluoride can be totally transformed to V_2O_5 and becomes stable.

To preliminary assess the practical value of such porous V_2O_5 layers we study their application in lithium-ion intercalation batteries as insertion host, which is one of the most promising applications of V_2O_5. We used crystallized V_2O_5 porous layers (annealing at 200 °C) directly as electrode, to test the lithium-ion battery performance (for experimental details see the Supporting Information). The lithium-ion charge/discharge process was investigated in a conventional electrolyte, that is, 1 M $LiPF_6$ in a 1:1 ethylene carbonate and diethyl carbonate mixture, with Li metal as the counter and reference electrodes. The potential window for galvanostatic charge/discharge processes was set between 2.7 and 4 V (vs. Li/Li^+). Within this potential window 1 mol of Li^+ is known to reversibly intercalate into 1 mol of V_2O_5, which corresponds to a maximum specific capacity of 148 mA h g^{-1}.[17] A typical charge/discharge profile obtained by a current density of 1/4 C (about 37 mA g^{-1}) at room temperature is shown in Figure 4. Two pairs of charge/discharge plateaus with high symmetry can be found from the

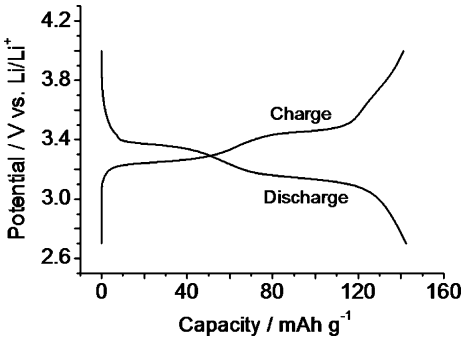

Figure 4. Lithium-ion galvanostatic charge/discharge curves of the porous V_2O_5 layer (anodically grown at 120 V for 1 h) at current densities of 1/4 C.

profiles which are due to the reversible phase transitions between different lithium-ion intercalated V_2O_5 phases.[18] A capacity of 142 mA h g^{-1} is obtained, that is, a coulombic efficiency of more than 99% can be achieved. Another promising property revealed by the porous V_2O_5 layer is the high cycling stability combined with a high energy density of around 450 Wh kg^{-1} (see Figure S9 in the Supporting Information) which are better than conventional V_2O_5 electrode materials.[19] Considering that these results are obtained with a structure which has a lot of room for optimization (length, annealing conditions) and the fact that the present findings can compete with the best reported nanostructured V_2O_5, gives this material a very promising perspective for use in lithium-ion intercalation devices. Another advantage of the highly ordered V_2O_5 porous layer is that it is directly grown on a conductive substrate, that is, it provides an easy operation for lithium-ion battery devices without addition of polymeric binders or graphitic particles to improve the electronic conduction in the electrode.[17]

In summary, we show that V_2O_5 layers with homogeneous nanoporous and nanotubular structures can successfully be fabricated by anodization of vanadium using complex fluoride-based electrolytes. The pore size and layer thickness can be controlled by the electrochemical conditions. These highly ordered V_2O_5 porous layers have a high potential for applications, for example, in lithium-ion batteries. Moreover, this simple and very successful approach may provide a new platform for growth of ordered oxide structures on transition metals where formation of self-organized oxide layers was not observed so far.

Experimental Section

Vanadium foils (0.25 mm, 99.8%, Advent Materials) were used as substrates, which were ground and polished to a mirror finish before use, followed by rinsing with deionized (DI) water and ethanol, respectively. Electrochemical anodization was carried out at room temperature in a solution of ethylene glycol (EG, Riedel-de Haën, 99.5%) with different amounts of HF, that is, from 0.1 to 0.6 M (40 vol%, Merck). Before anodization, metallic titanium with different concentrations from 200 to 2000 ppm was dissolved in the solution to introduce $[TiF_6]^{2-}$ ions in the electrolyte. As control experiments, other buffer species such as $(NH_4)_2TiF_6$ (Sigma–Aldrich, 99.99%), NH_4BF_4 (Sigma–Aldrich, 99.99%), and $NaBF_4$ (Sigma–Aldrich, $\geq$98.0%) were used (7 mM $(NH_4)_2TiF_6$ with 0.1 M HF, 14 mM NH_4BF_4 or $NaBF_4$ with 3 M H_2O in ethylene glycol). Other control experiments were done by dissolving V of different concentrations in the fluoride electrolyte. Anodization was conducted at different potentials from 40 to 300 V for certain duration to grow nanoporous layers. Experiments were carried out at room temperature in a two-electrode set-up with platinum gauze as a counter electrode. After anodization, the samples were immersed in ethanol overnight followed by annealing at 200 °C for 3 h in air. A field-emission scanning electron microscope (Hitachi FE-SEM S4800) equipped with an energy dispersive X-ray (EDX) analyzer was used to investigate the morphology and composition of the samples. The crystal structure of the sample was evaluated using X-ray diffraction (XRD) analysis which was performed by an X′pert Phillips PMD with a PANalytical X′celerator detector using graphite-monochromatized CuKα radiation. Additional investigation on the composition and chemical states of the anodic layers was obtained from using X-ray photoelectron spectroscopy (XPS, PHI 5600, PerkinElmer). Lithium-ion insertion experiments were performed as discussed in the Supporting information (Figure S9).

Received: June 12, 2011
Revised: August 4, 2011
Published online: August 26, 2011

Keywords: electrochemistry · microporous materials · nanotubes · oxidation · vanadium

[1] H. Masuda, K. Fukuda, *Science* **1995**, *268*, 1466.
[2] a) B. B. Lakshmi, P. K. Dorhout, C. R. Martin, *Chem. Mater.* **1997**, *9*, 857; b) G. E. Thompson, *Thin Solid Films* **1997**, *297*, 192; c) H. Masuda, M. Ohya, H. Asoh, M. Nakao, M. Nohtomi, T. Tamamura, *Jpn. J. Appl. Phys.* **1999**, *38*, L1403; d) S. Shingubara, *J. Nanopart. Res.* **2003**, *5*, 17.
[3] V. Zwilling, E. Darque-Ceretti, A. Boutry-Forveille, D. David, M. Y. Perrin, M. Aucouturier, *Surf. Interface Anal.* **1999**, *27*, 629.
[4] a) J. M. Macák, H. Tsuchiya, P. Schmuki, *Angew. Chem.* **2005**, *117*, 2136; *Angew. Chem. Int. Ed.* **2005**, *44*, 2100; b) J. M. Macak, H. Tsuchiya, L. Taveira, S. Aldabergerova, P. Schmuki, *Angew. Chem.* **2005**, *117*, 7629; *Angew. Chem. Int. Ed.* **2005**, *44*, 7463.
[5] a) S. P. Albu, A. Ghicov, J. M. Macak, P. Schmuki, *Phys. Status Solidi RRL* **2007**, *1*, R65; b) J. Park, S. Bauer, K. von der Mark, P. Schmuki, *Nano Lett.* **2007**, *7*, 1686; c) S. P. Albu, D. Kim, P. Schmuki, *Angew. Chem.* **2008**, *120*, 1942; *Angew. Chem. Int. Ed.* **2008**, *47*, 1916; d) D. Kim, A. Ghicov, S. P. Albu, P. Schmuki, *J. Am. Chem. Soc.* **2008**, *130*, 16454; e) A. Ghicov, P. Schmuki, *Chem. Commun.* **2009**, 2791; f) K. Lee, D. Kim, P. Roy, I. Paramasivam, B. I. Birajdar, E. Spiecker, P. Schmuki, *J. Am. Chem. Soc.* **2010**, *132*, 1478.
[6] a) P. Liu, S. H. Lee, C. E. Tracy, Y. Yan, J. A. Turner, *Adv. Mater.* **2002**, *14*, 27; b) J. Döbler, M. Pritzsche, J. Sauer, *J. Am. Chem. Soc.* **2005**, *127*, 10861; c) J. Liu, X. Wang, Q. Peng, Y. Li, *Adv. Mater.* **2005**, *17*, 764; d) C. Xiong, A. E. Aliev, B. Gnade, K. J. Balkus, Jr., *ACS Nano* **2008**, *2*, 293.
[7] a) A. Chakrabarti, K. Hermann, R. Druzinic, M. Witko, F. Wagner, M. Petersen, *Phys. Rev. B* **1999**, *59*, 10583; b) A. Augustsson, T. Schmitt, L. C. Duda, J. Nordgren S. Nordlinder, K. Edström, T. Gustafsson, J. H. Guo, *J. Appl. Phys.* **2003**, *94*, 5083; c) D. Sun, C. W. Kwon, G. Baure, E. Richman, J. MacLean, B. Dunn, S. H. Tolbert, *Adv. Funct. Mater.* **2004**, *14*, 1197.
[8] a) M. E. Spahr, P. Bitterli, R. Nesper, M. Müller, F. Krumeich, H. U. Nissen, *Angew. Chem.* **1998**, *110*, 1339; *Angew. Chem. Int. Ed.* **1998**, *37*, 1263; b) F. Krumeich, H. J. Muhr, M. Niederberger, F. Bieri, B. Schnyder, R. Nesper, *J. Am. Chem. Soc.* **1999**, *121*, 8324; c) L. Kavan, M. Kalbáč, M. Zukalová, I. Exnar, V. Lorenzen, R. Nesper, M. Graetzel, *Chem. Mater.* **2004**, *16*, 477.
[9] a) J. P. Schreckenbach, P. Strauch, *Appl. Surf. Sci.* **1999**, *143*, 6; b) G. B. Stefanovich, A. L. Pergament, A. A. Velichko, L. A. Stefanovich, *J. Phys. Condens. Matter* **2004**, *16*, 4013.
[10] a) R. G. Keil, R. E. Salomon, *J. Electrochem. Soc.* **1968**, *115*, 628; b) S. Hornkjøl, I. M. Hornkjøl, *Electrochim. Acta* **1991**, *36*, 577; c) W. B. Fan, D. Kirkwood, J. W. Lu, S. A. Wolf, *Appl. Phys. Lett.* **2009**, *95*, 232110.
[11] a) A. Ghicov, H. Tsuchiya, J. M. Macak, P. Schmuki, *Electrochem. Commun.* **2005**, *7*, 505; b) J. M. Macak, K. Sirotna, P. Schmuki, *Electrochim. Acta* **2005**, *50*, 3679; c) S. Bauer, S. Kleber, P. Schmuki, *Electrochem. Commun.* **2006**, *8*, 1321.
[12] a) A. Ghicov, S. Aldabergerova, H. Tsuchiya, P. Schmuki, *Angew. Chem.* **2006**, *118*, 7150; *Angew. Chem. Int. Ed.* **2006**, *45*, 6993; b) P. Roy, S. Berger, P. Schmuki, *Angew. Chem.* **2011**, *123*, 2956; *Angew. Chem. Int. Ed.* **2011**, *50*, 2904; c) S. P. Albu, P. Roy, S. Virtanen, P. Schmuki, *Isr. J. Chem.* **2010**, *50*, 453.
[13] J. Mendialdua, R. Casanova, Y. Barbaux, *J. Electron Spectrosc. Relat. Phenom.* **1995**, *71*, 249.

[14] a) C. M. Zheng, X. M. Zhang, Z. P. Qiao, D. M. Lei, *J. Solid State Chem.* **2001**, *159*, 181; b) Y. T. Kim, S. Gopukumar, K. B. Kim, B. W. Cho, *J. Power Sources* **2003**, *117*, 110.
[15] I. Bányai, V. Conte, L. Pettersson, A. Silvagni, *Eur. J. Inorg. Chem.* **2008**, *34*, 5373.
[16] M. C. Chakravorti, A. R. Sarkar, *J. Fluorine Chem.* **1976**, *8*, 255.
[17] C. R. Sides, C. R. Martin, *Adv. Mater.* **2005**, *17*, 125.
[18] N. A. Chernova, M. Roppolo, A. C. Dillon, M. S. Whittingham, *J. Mater. Chem.* **2009**, *19*, 2526.
[19] a) J. M. Cocciantelli, M. Menetrier, C. Delmas, J. P. Doumerc, M. Pouchard, M. Broussely, J. Labat, *Solid State Ionics* **1995**, *78*, 143; b) Y. Wang, K. Takahashi, K. Lee, G. Z. Cao, *Adv. Funct. Mater.* **2006**, *16*, 1133.

